Structure Determination and Characterization of *Saccharomyces cerevisiae* Profilin†

Janina C. Eads,‡,§ Nicole M. Mahoney,‡ Sergey Vorobiev,‡ Anne R. Bresnick,‡ Kuo-Kuang Wen,|| Peter A. Rubenstein,|| Brian K. Haarer,⊥ and Steven C. Almo*,‡

Department of Biochemistry, Albert Einstein College of Medicine, Bronx, New York 10461, Department of Biochemistry, University of Iowa, Iowa City, Iowa 52242-1193, and Department of Zoology, University of Texas, Austin, Texas 78712

Received August 12, 1997; Revised Manuscript Received May 16, 1998

ABSTRACT: The structure of profilin from the budding yeast *Saccharomyces cerevisiae* has been determined by X-ray crystallography at 2.3 Å resolution. The overall fold of yeast profilin is similar to the fold observed for other profilin structures. The interactions of yeast and human platelet profilins with rabbit skeletal muscle actin were characterized by titration microcalorimetry, fluorescence titrations, and nucleotide exchange kinetics. The affinity of yeast profilin for rabbit actin (2.9 μM) is approximately 30-fold weaker than the affinity of human platelet profilin for rabbit actin (0.1 μM), and the relative contributions of entropic and enthalpic terms to the overall free energy of binding are different for the two profilins. The titration of pyrene-labeled rabbit skeletal actin with human profilin yielded a K_d of 2.8 μM, similar to the K_d of 2.0 μM for the interaction between yeast profilin and pyrene-labeled yeast actin. The binding data are discussed in the context of the known crystal structures of profilin and actin, and the residues present at the actin−profilin interface. The affinity of yeast profilin for poly-L-proline was determined from fluorescence measurements and is similar to the reported affinity of *Acanthamoeba* profilin for poly-L-proline. Yeast profilin was shown to catalyze adenine nucleotide exchange from yeast actin almost 2 orders of magnitude less efficiently than human profilin and rabbit skeletal muscle actin. The in vivo and in vitro properties of yeast profilin mutants with altered poly-L-proline and actin binding sites are discussed in the context of the crystal structure.

Profilin (13−15 kDa) is a regulatory component of the actin cytoskeleton in all eukaryotic cells (*1*−*4*), which binds monomeric actin (G-actin) with an in vitro equilibrium dissociation constant (K_d) in the micromolar to sub-micromolar range (*5*−*7*). In vivo, profilin has been proposed to regulate the formation of specific F-actin structures by several mechanisms, including actin monomer sequestration (*5*), enhancement of actin-bound nucleotide exchange (*8*, *9*), and the ability to couple actin monomer addition at the barbed end of an elongating filament with ATP hydrolysis (*10*).

Polyphosphoinositides such as phosphatidylinositol 4,5-bisphosphate (PIP_2)[1] inhibit the actin-associated activities of profilin by disrupting the profilin−actin complex (*11*). This is thought to be due to direct steric competition, as genetic and structural studies suggest that the PIP_2 and actin binding sites of profilin overlap (*12*−*14*). Furthermore, profilin inhibits the phospholipase C_γ-catalyzed hydrolysis of PIP_2 to IP_3 and diacylglycerol (*15*), thus providing a possible link between the PIP_2 signaling pathway and the reorganization of the actin cytoskeleton. Recently, profilin has been suggested to activate PI3 kinase through interaction with the 85 kDa regulatory domain, further connecting profilin with phosphoinositide metabolism (*16*).

All cellular profilins bind proline-rich sequences in peptides and proteins via a patch of five highly conserved hydrophobic residues on the surface of the molecule (*17*−*21*). Mammalian profilins colocalize with the focal-adhesion proteins VASP (vasodilator-stimulated phosphoprotein) and MENA (mammalian homologue of *Drosophila enabled*), which are involved in F-actin assembly, and which both contain multiple proline-rich sequences (*22*−*24*). Profilin has also been shown to interact in vitro and in vivo with members of the formin family (*25*−*28*), a group of proline-rich proteins involved in a variety of developmental and morphological processes. For example, Bni1p, a formin homologue from *Saccharomyces cerevisiae*, binds to profilin in vitro, and *bni1* mutants are unable to regulate the spatial and temporal localization of specific F-actin structures in vivo (*25*). The interaction of profilin with proline-rich proteins provides a mechanism for localizing profilin and its actin-related activities to sites requiring actin filament assembly.

Many of the in vivo studies addressing profilin function have utilized mutants of the budding yeast *S. cerevisiae*. In

† This work was supported by NIH Grants GM33689 to P.A.R. and GM53807 to S.C.A.

* To whom correspondence should be addressed: Department of Biochemistry, Albert Einstein College of Medicine, 1300 Morris Park Ave., Bronx, NY 10461. Phone: (718) 430-2746. E-mail: almo@aecom.yu.edu.

‡ Albert Einstein College of Medicine.

§ Present address: School of Biochemistry, University of Birmingham, Edgbaston, Birmingham B15 2TT, U.K.

|| University of Iowa.

⊥ University of Texas.

[1] Abbreviations: ATP, adenosine 5′-triphosphate; ADP, adenosine 5′-diphosphate; DTT, dithiothreitol; HEPES, *N*-(2-hydroxyethyl)piperazine-*N*′-2-ethanesulfonic acid; HPP, human platelet profilin; ITC, isothermal titration calorimetry; NCS, noncrystallographic symmetry; PCR, polymerase chain reaction; PIP_2, phosphatidylinositol bisphosphate; MOPS, 3-(*N*-morpholino)propanesulfonic acid; Tris, tris(hydroxymethyl)aminomethane.

S0006-2960(97)02003-5 CCC: $15.00
Published on Web 07/21/1998

S. cerevisiae, as well as in several other organisms, profilin is involved in establishing and maintaining a normal distribution of actin structures (*1*−*4*). In wild type *S. cerevisiae*, the actin cytoskeleton is organized into cables that run longitudinally across the cell and cortical actin patches in regions of active growth (*29*, *30*). Profilin null strains of *S. cerevisiae* have an altered distribution of actin structures, often displaying a single thick bar of actin, a random distribution of cortical actin patches, and an absence of actin cables. This is accompanied by altered morphology and temperature sensitivity and the frequent occurrence of multinucleate cells (*1*). In this paper, we report the three-dimensional structure of *S. cerevisiae* profilin, hereafter referred to as yeast profilin, and new data characterizing the interactions of yeast and human profilins with yeast and rabbit skeletal muscle actin.

MATERIALS AND METHODS

Overexpression and Purification of S. cerevisiae and Human Platelet Profilin. PCR was used to introduce the coding region of yeast profilin into the *Nde*I and *Eco*RI sites of pMW172, a pET derivative. The resultant construct was transformed into *Escherichia coli* BL21(DE3) (Novagen). After growth at 37 °C, single colonies were selected and grown for 8 h in 5 mL of LB media with 100 μg/mL carbenicillin and were used to inoculate 4 × 500 mL of LB media. Cultures were grown overnight at 32 °C and the cells harvested by centrifugation, frozen at −80 °C, thawed, and resuspended in 50−75 mL of cracking buffer [0.1 M Tris (pH 8), 40 mM KCl, 1 mM DTT, and l mM PMSF] which contained a cocktail of protease inhibitors supplied in tablet form from Boehringer (Complete). Lysozyme was added to a final concentration of 0.2 mg/mL, and the mixture was stirred for 30 min. The slurry was sonicated in four or five bursts of 15 s each and then centrifuged in a Ti45 rotor at 37 000 rpm for 1 h. The supernatant was filtered using a 0.2 μM particle filter (Nalgene) and applied directly to a poly-L-proline affinity column equilibrated with buffer TK8 [10 mM Tris (pH 8), 40 mM KCl, and l mM DTT]. The column was washed with 6−10 column volumes of buffer TK8, followed by 5−7 column volumes of 2.5 M urea in TK8. Profilin was eluted from the column with 8 M urea. Fractions containing profilin were pooled and dialyzed against buffer TK8 and concentrated to 10−30 mg/mL by Amicon ultrafiltration. Human platelet profilin (HPP) was overexpressed and purified by poly-L-proline affinity chromatography as previously described (*31*). The profilins were judged to be >95% pure by SDS−PAGE and were stored at 0 °C until they were required. Birch pollen profilin was purified by poly-L-proline affinity chromatography as previously described (*32*). The concentrations of both human platelet and yeast profilin were determined spectrophotometrically, using an ϵ_{280} of 20 300 M^{-1} cm^{-1} for yeast profilin and an ϵ_{280} of 17 960 M^{-1} cm^{-1} for human platelet profilin. The extinction coefficient for yeast profilin was determined by quantitative amino acid analysis and is consistent with the predicted value for yeast profilin. The molecular mass of purified recombinant yeast profilin was determined by mass spectroscopic analysis. The observed mass, 13 547 Da, is within 1 Da of the predicted mass for yeast profilin without the N-terminal methionine.

Purification and Pyrenylation of Yeast and Rabbit Skeletal Muscle Actin. Actin was purified from rabbit muscle acetone powder by the method of Spudich and Watt (*33*) and gel filtered (Sephacryl S-300, Pharmacia Biotech). The fractions corresponding to monomeric actin were pooled and stored at 2−4 °C in dialysis against buffer A [2 mM Tris (pH 8), 0.2 mM ATP, 0.5 mM DTT, 0.1 mM $CaCl_2$, and l mM NaN_3]. The actin concentration was determined spectrophotometrically using an A_{290} of 0.63 for a 1 mg/mL solution. Pyrene-labeled rabbit skeletal muscle actin was prepared by reaction with *N*-(1-pyrenyl)iodoacetamide (Molecular Probes Inc.) (*34*). Yeast actin was prepared from yeast cakes by a modification of a previously described protocol (*35*). Briefly, clarified cell lysates were applied to a DNase I affinity column, and actin was eluted with 50% formamide and applied directly to a DEAE anion exchange column. The actin was eluted with 0.5 M KCl, dialyzed overnight against buffer A, polymerized by the addition of 4 mM $MgCl_2$ and 50 mM KCl, and pelleted by centrifugation. The pellet was resuspended in buffer A and dialyzed against three changes of buffer over 2 days. The actin was clarified by centrifugation to remove higher-order aggregates and only the top two-thirds used for subsequent experiments. Yeast actin was modified with *N*-(1-pyrenyl)maleimide (Sigma) for fluorescence titrations.

Crystallization and Data Collection. Crystals of yeast profilin were grown by the hanging drop vapor diffusion method. Yeast profilin (5−8 mg/mL) was mixed with an equal volume of a precipitant solution and suspended on a silanized cover slip above 1 mL of the same solution. Two crystal forms were obtained from an initial screen of crystallization conditions. A cubic crystal form was obtained using a reservoir solution containing 3.8−4.0 M sodium formate, and a hexagonal crystal form was obtained using a reservoir solution containing 1.0 M lithium sulfate, 0.1 M Tris (pH 8.5), and 0.01 M $NiCl_2$. The cubic crystal form diffracted to 2.8 Å resolution, yielding a diffraction pattern consistent with space group *P*432, with the following unit cell dimensions: $a = b = c = 129.17$ Å and $\alpha = \beta = \gamma = 90°$. The hexagonal crystal form diffracted to higher resolution (2.2 Å) and was used for structure determination and refinement.

Two native data sets were collected for the hexagonal crystal form at room temperature using a Siemens X-1000 area detector, with a Rigaku RU-200 rotating anode as the X-ray source. Data were processed with either XDS (*36*) or XENGEN (*37*). Diffraction from the crystals was consistent with the hexagonal space group $P6_1$ or $P6_5$ ($a = b = 58.1$, $c = 151.3$, $\alpha = \beta = 90°$, and $\gamma = 120°$), with two molecules of yeast profilin in the asymmetric unit (53% solvent). Statistics for the higher-resolution data set used for final refinement of the structure are given in Table 1.

Structure Determination and Refinement. The structure was solved by molecular replacement using the program AMORE (*38*), as part of the CCP4 suite of programs (*39*). The search model was the 2 Å refined structure of *Acanthamoeba* profilin isoform I (*13*), with side chains but with no ordered solvent. A rotation search did not yield a clear solution, so the top seven solutions were used in a translation search in space groups $P6_1$ and $P6_5$. The translation function in $P6_5$ yielded a distinct solution, which was fixed while a second translation search was performed to locate the second

Table 1: Structure Solution

Data Collection and Reduction	
space group	$P6_5$
unit cell parameters (Å)	$a = b = 58.1$, $c = 151.3$
resolution range	$\infty \rightarrow 2.3$ Å
no. of unique reflections	12 068
completeness of data (%)	93
data redundancy	3.7
R_{sym} (R_{sym} in the 2.4−2.3 Å shell) (%)	6.4 (21.3)
Refinement Statistics	
resolution range (Å)	15−2.3
R-factor (R_{free}) (%)	16.8 (22.0)
rms deviations from ideal geometry	
bond lengths (Å)	0.009
bond angles (deg)	1.5
no. of protein atoms	1912
no. of solvent atoms	39
average temperature factors (Å^2)	
molecule A	30.3
molecule B	38.0
solvent	34.3

molecule in the asymmetric unit. There was a clear solution for the second molecule, and the two solutions were subjected to rigid-body refinement with AMORE, resulting in an R-factor of 46% (R_{free} = 43.9%) for data between 10 and 3 Å. At this stage, the side chains of the model were removed, leaving a poly(alanine-glycine) structure. This new model was subjected to simulated annealing from 3000 K and positional refinement, with the application of noncrystallographic symmetry (NCS) restraints with X-PLOR (*40*). Electron density maps calculated with the refined poly(alanine-glycine) model showed clear electron density for many side chains of yeast profilin; these were added to the model using the interactive graphics program O (*41*). After two rounds of model building and simulated annealing refinement, the model was refined using positional and grouped B-factor refinement with NCS restraints applied. Using data to 2.7 Å with a 2σ cutoff, an R-factor of 20% (R_{free} = 26.6%) was obtained. Subsequently, a higher-resolution data set was obtained and used for further refinement; the test set of reflections used for calculation of R_{free} was kept constant for the overlapping resolution range, adding extra test reflections between 2.7 and 2.3 Å. Rigid-body refinement followed by positional and individual B-factor refinement without NCS restraints reduced the R-factor to 18.7% (R_{free} = 23.0%) for data to 2.3 Å. A final round of model building, in which 39 water molecules were added to the model, was followed by positional and B-factor refinement, yielding a final model with an R-factor of 16.8% (R_{free} = 22.0%), with excellent model geometry (Table 1). Typical electron density is shown in Figure 1, in which the final $(2|F_o| - |F_c|)\phi_c$ map is shown for residues 1−12 (i.e., α1) of the final model of yeast profilin. The refined coordinates of yeast profilin have been deposited with the Brookhaven Protein Data Bank (PDB entry 1YPR).

Titration Microcalorimetry. Isothermal titration calorimetry (ITC) experiments were carried out using a MicroCal Omega isothermal titration calorimeter (MicroCal Inc.). Purified rabbit muscle actin (60−100 μM) was titrated with concentrated solutions of human platelet or yeast profilin (0.8−1.0 mM). Both proteins were extensively dialyzed against the buffer used for each experiment, and the final dialysate was used for concentration adjustments and control titrations of profilin into buffer. A low-ionic strength buffer composed of 2 mM buffer (Tris, PIPES, MOPS, or cacodylate), 0.2 mM ATP, 0.5 mM DTT, 0.1 mM $CaCl_2$, and 1 mM NaN_3 was used in all experiments. Typically, profilin was injected into actin using 20 injections of 12.5 μL each, with 3 min between each injection. The contents of the sample cell (1.34 mL working volume) was stirred at 350 rpm during the experiment. All measurements were conducted at 27 °C. Each titration peak was integrated manually using the data before and after each peak to establish a baseline. Data analysis to determine the thermodynamic parameters of actin−profilin binding was performed with the Origin software package (MicroCal Inc.), which uses a nonlinear interactive Marquardt method to fit the data. A single-site model was assumed. Where the heat of dilution of profilin into buffer was non-negligible, a control titration of profilin into buffer was performed. The control gave a small linear decrease in enthalpy with each injection, and the best straight line through the control data points was subtracted from the actin−profilin titration data.

Stopped-Flow Kinetics. Fluorescence measurements of actin nucleotide exchange were performed using an Applied Photophysics SX.17MV stopped-flow spectrophotometer operated in the fluorescence mode at 20 °C. The human and yeast actins were diluted to a concentration of 4 μM with buffer A lacking ATP. Actin in either the presence or absence of yeast, birch pollen, or human profilin was rapidly mixed with an equal volume of buffer A containing 200 μM ϵATP and no additional ATP. The increase in fluorescence intensity due to the binding of ϵATP to actin was monitored at wavelengths above 392 nm, using excitation at 360 nm and a 392 nm cutoff filter on the emission. The final concentration of bona fide ATP was less than 8 μM. The time course of the emission kinetics was fit to a single-exponential function using the GLINT (Applied Photophysics) program to determine the observed nucleotide dissociation rate constant (k_{obs}).

Measurement of Pro_{50} Binding. Yeast profilin (2 μM) in TK8 buffer was prepared with different concentrations of Pro_{50}. Proline concentrations were determined spectrophotometrically using an ϵ_{204} of 5.63×10^3 M^{-1} cm^{-1} (*42*). Fluorescence measurements were conducted at 22 °C, using a Perkin-Elmer LS-5B spectrophotometer. The excitation wavelength was 295 nm (10 nm slit width), and the emission intensity was monitored at 318 nm (3 nm slit width). The data were fit by a nonlinear least-squares method using the Kaleidagraph fitting program.

Urea Denaturation. Yeast profilin (2.5 μM) in TK8 buffer was incubated with different concentrations of urea at 20 °C for 30 min. The fluorescence emission of each sample was monitored at 370 nm, with excitation at 295 nm, with instrumentation as described above. Three independent sets of experiments were normalized and averaged.

Fluorescence Titrations. The fluorescence enhancement of pyrene-labeled yeast and rabbit skeletal muscle actin was used to measure the binding of yeast and human profilin. Binding assays were performed with 1 μM pyrene-labeled actin (100%) and varying amounts of the profilins in buffer A at 25 °C. The excitation wavelength was 344 nm, and the emission intensity was monitored at 385 nm. The data were fit to the Michaelis−Menten equation to derive equilibrium dissociation constants.

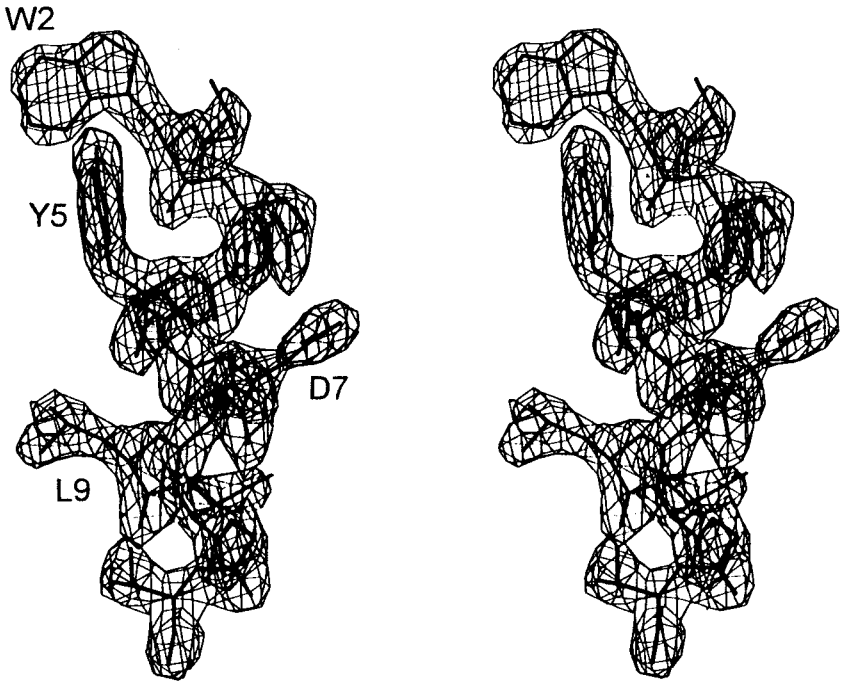

FIGURE 1: Electron density map ($2F_c - F_c$) in the N-terminal region of yeast profilin, contoured at 1.5σ. The final refined coordinates of residues 1−12 of yeast profilin are shown in stick representation.

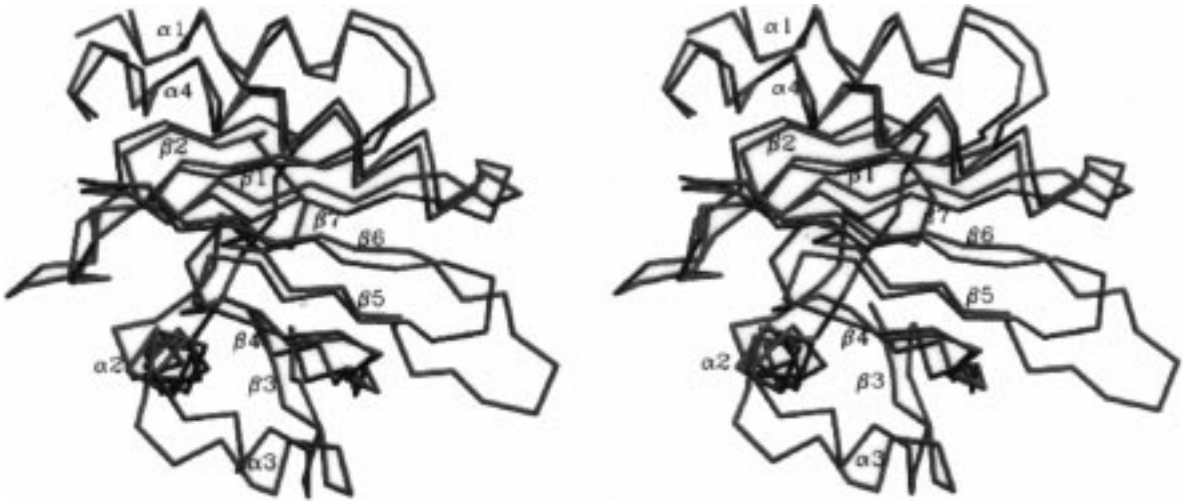

FIGURE 2: Overlay of C_α traces of yeast and human profilin structures. Blue is human; pink is yeast. Alignment of the corresponding C_α atoms of yeast and *Acanthamoeba* profilins gives an rms deviation of 1.1 Å for superposition of 112 C_α atoms, whereas alignment of the major secondary structural elements of human profilin with yeast profilin gives an rms deviation of 1.6 Å over 110 C_α atoms.

RESULTS

Overall Fold of Yeast Profilin. The overall fold of yeast profilin is similar to that observed for the *Acanthamoeba* (*13*) and mammalian profilins (*14*, *21*, *43*; A. A. Fedorov and S. C. Almo, unpublished results; PDB entry 1FIL) (Figure 2). All of the secondary structural elements observed in the crystal structures of the profilins are conserved, except for the variation in the N-terminal α-helix. In the yeast profilin structure,[2] the N-terminal helix extends from residue 1 to 11 before terminating in a loop which leads into a β-sheet, whereas in the *Acanthamoeba* profilin structure, the N-terminal α-helix ends with a turn of noncanonical helix in which i to $i + 5$ main chain hydrogen bonds are formed (*13*). Thus, yeast profilin consists of a central six-stranded antiparallel β-sheet composed of β1 (17−22), β2 (27−32), β4 (65−73), β5 (76−81), β7 (84−91), and β8 (94−100). The N-terminal helix α1 (1−11) and C-terminal helix α4 (106−123) are on one side of this sheet and run approximately parallel to the β-strands. On the other side of the central sheet are two helices, α2 (39−50) and α3 (53−58), and a short two-stranded sheet consisting of strand β3 (60−62) and the first three residues of strand β4. Strand β4 has a sharp bend (β-bulge) at Leu70 which allows it to participate in both β-sheets. Alignment of the corresponding C_α atoms of yeast and *Acanthamoeba* profilins gives an rms deviation of 1.1 Å for superposition of 112 C_α atoms, whereas alignment of the major secondary structural elements of human profilin with yeast profilin gives an rms deviation

[2] The yeast profilin is numbered from residue 1 to 125. The initiator methionine is absent from the recombinant yeast profilin; thus, serine is residue 1.

Table 2: Thermodynamic Parameters for Binding of Profilins to Rabbit Muscle Actin, Obtained from ITC Data

	S. cerevisiae profilin	human platelet profilin
K_d (μM)[a]	2.9 ± 0.7	0.1 ± 0.02
ΔG (kcal/mol)	−7.6	−9.6
ΔH_{react} (kcal/mol)[b]	−12.1	−3.4
$T\Delta S$ (kcal/mol)	−4.5	6.2
N_{H^+}[b]	0.86 ± 0.05[c]	0.1 ± 0.1[c]

[a] Average value obtained from measurements in different buffers; error is the standard deviation of the average. [b] Values obtained from a plot of ΔH_{bind} vs ΔH_{ion} (Figure 5 for yeast profilin). ΔH_{react} is the intrinsic enthalpy of the binding reaction. N_{H^+} is the number of protons released by the buffer to the complex on binding of actin to profilin. For the HPP−actin interaction, ΔH_{bind} was measured in Tris and PIPES buffers only. [c] Estimated error.

of 1.6 Å for 110 C_α atoms. The C_α trace of yeast profilin is shown in Figure 2, superimposed on the C_α trace of human profilin. Two loops in the mammalian profilins are longer than their counterparts in other profilins, including yeast profilin. Between strands β4 and β5, and β5 and β6, there are five and six additional residues, respectively, in human profilin, compared to yeast profilin.

The two independent molecules of yeast profilin are related by a noncrystallographic symmetry axis which is not a proper 2-fold axis; the angle relating the two molecules (κ) is 67° (polar angles). The dimer does not appear to be of any physiological significance, as the two molecules in the asymmetric unit do not share a substantial interface, although there are close lattice contacts with symmetry-related molecules. The two molecules of yeast profilin in the asymmetric unit of the crystal are very similar with an rms deviation of 0.48 Å for all C_α atoms; however, there are some slight differences in the two molecules which are most likely a result of lattice effects. This is most apparent in the difference in the average *B*-factor for the two molecules; for molecule A, $\langle B \rangle = 30$ Å^2, whereas for molecule B, $\langle B \rangle = 38$ Å^2. In particular, residues 36−40 leading into the start of helix α2 are disordered in molecule B, showing high *B*-factors, whereas in molecule A, the temperature factors for these residues are not significantly above the average. In molecule A, these residues pack against residues 50−57 of a symmetry-related molecule, thus restraining localized motions, whereas in molecule B, these residues do not make any lattice contacts. A Ramachandran plot shows that with the exception of Asp82, all residues fall within conformationally allowed regions (data not shown). Asp82 is in a type II′ turn, and shows good electron density in molecule B, but not in molecule A.

Thermodynamic Characterization of the Profilin−Actin Interaction. The thermodynamic data obtained for the interaction of rabbit muscle actin with yeast and human profilin are listed in Table 2. A typical titration of yeast profilin with rabbit actin is shown in Figure 3B, with the integrated area of each peak corrected for the heat of dilution of profilin into buffer shown in Figure 3C. The data show that both profilins bind to actin with a 1:1 stoichiometry. The integrated and corrected peak areas were analyzed by a nonlinear least-squares fitting routine to derive ΔH_{bind}, K_d, and the stoichiometry of the reaction, where ΔH_{bind} is the measured enthalpy of the binding reaction, including contributions from the ionization of the buffer due to proton uptake or release during the reaction. The binding of human profilin to rabbit skeletal muscle actin based on calorimetry is characterized by a K_d of 0.1 μM, while the K_d for the yeast profilin is 2.9 μM. Fluorescence titration using pyrene-labeled yeast actin yielded K_d values of 2.0 and 5.4 μM for yeast and human profilin, respectively (Figure 4 and Table 3). Fluorescence titration using pyrene-labeled rabbit skeletal muscle actin yielded K_d values of 18.2 and 2.8 μM for yeast and human profilin, respectively (Table 3).

Measurement of the binding enthalpy (ΔH_{bind}) in buffers with different heats of ionization allowed for the determination of the intrinsic enthalpy of the actin−profilin interaction (ΔH_{react}) and the net number of protons (N_{H^+}) transferred between the buffer and complex (i.e., proton linkage) (*44*). The ΔH_{bind} values for the actin−yeast profilin interaction measured in different buffers are plotted in Figure 5, and the intercept at $\Delta H_{ion} = 0$ gives an intrinsic ΔH_{react} of −12.1 kcal/mol (Table 2). The slope of the plot in Figure 5 is 0.86, showing that on binding of yeast profilin to rabbit actin, 0.86 protons are transferred from the buffer to the complex in the pH range of 7.2−8 (Table 2). The human profilin−rabbit actin interaction had a much smaller proton linkage (data not shown), as it was estimated that 0.1 (i.e., close to zero) protons are transferred from the buffer upon complex formation (Table 2). The values of ΔG and $T\Delta S$ were calculated from the measured values of ΔH and K_d (Table 2).

Kinetics of Actin Nucleotide Exchange. Figure 6 shows the time course of ϵATP binding to rabbit skeletal muscle actin, as monitored by the increase in ϵATP fluorescence. The nucleotide exchange kinetics were monitored in the absence and presence of yeast, human platelet profilin, or birch pollen profilin. The observed rate constants for nucleotide exchange from rabbit skeletal actin were calculated using a single-exponential fit to the data and were found to be 2.99×10^{-3} s^{-1} for actin alone, 8.80×10^{-3} s^{-1} in the presence of 100 μM yeast profilin, and 7.74×10^{-1} s^{-1} in the presence of 10 μM human platelet profilin. The observed rate constants for nucleotide exchange from yeast actin were found to be 6.02×10^{-3} s^{-1} for actin alone, 1.79×10^{-2} s^{-1} in the presence of 100 μM yeast profilin, 5.08×10^{-3} s^{-1} in the presence of 40 μM birch pollen profilin, and 5.38×10^{-3} s^{-1} in the presence of 80 μM birch pollen profilin. These results are summarized in Table 4.

*Binding of Poly-*L*-proline to Yeast Profilin.* The fluorescence enhancement observed on binding of poly-L-proline to yeast profilin was used to determine the K_d of the interaction. The raw data and curve fit are shown in Figure 7. The best fit gives a K_d value of 5.5 μM for Pro_{50} binding to yeast profilin, which corresponds to a K_d of 276 μM per proline residue.

Urea Denaturation. The denaturation of yeast profilin in urea was measured by monitoring the change in fluorescence at 370 nm. The fluorescence data are shown in Figure 8. The midpoint for the urea-induced transition is approximately 3.4 M, which is similar to the previously reported value of 3.5 M for *Acanthamoeba* profilin (*45*) measured under identical conditions. Linear extrapolation of the data to zero urea concentration yielded a free energy for unfolding of 5.9 kcal/mol and an *m* of 1.8 kcal/mol^2. The free energy of unfolding for *Acanthamoeba* profilin has been reported to be 7.6 kcal/mol (*18*). The observed difference may reflect

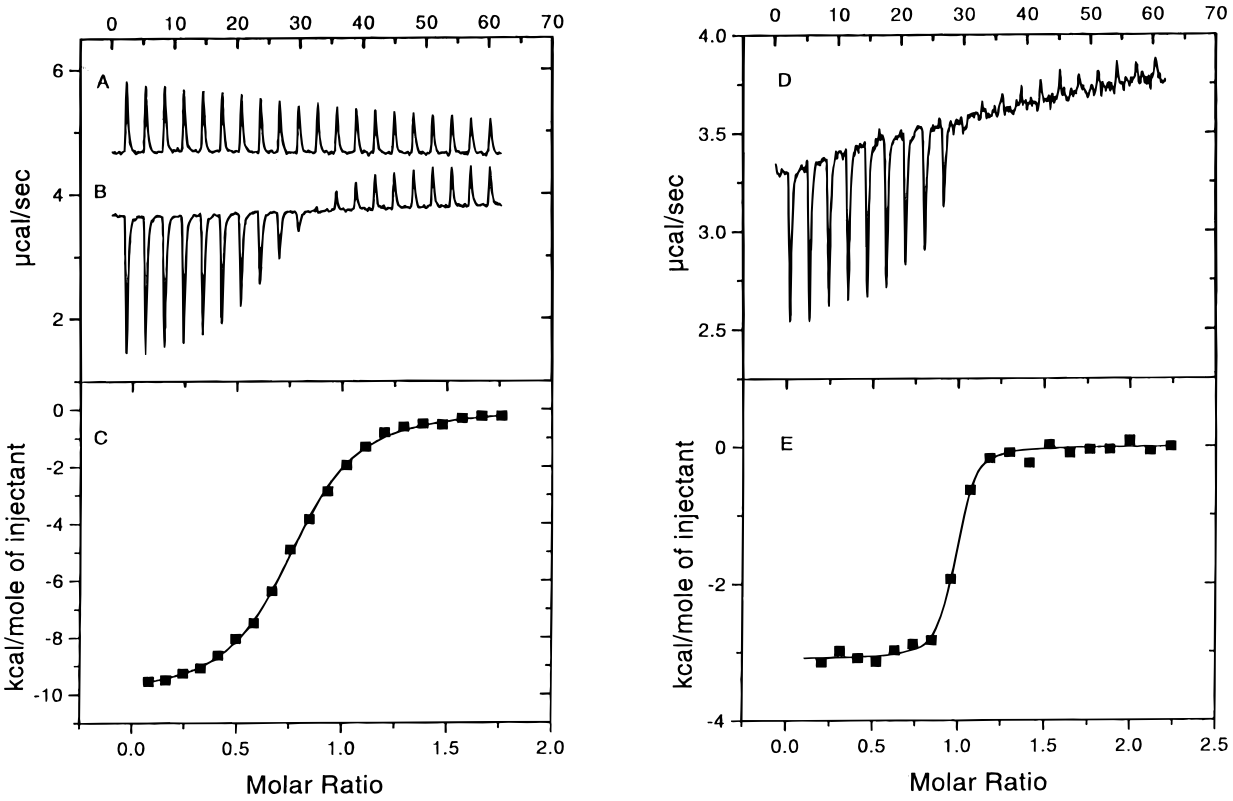

FIGURE 3: (A) Control ITC data for injections of 848 μM yeast profilin into buffer. (B) Raw ITC data for injections of 848 μM yeast profilin into 70 μM rabbit actin in 2 mM PIPES buffer (pH 7.2) containing 2 mM ATP, 0.1 mM $CaCl_2$, and 0.5 mM DTT. (C) Corrected, integrated data, with a curve fit for yeast profilin−actin data. (D) Raw ITC data for injections of 704 μM human platelet profilin into 64 μM rabbit actin in 2 mM PIPES buffer (pH 7.2) containing 2 mM ATP, 0.1 mM $CaCl_2$, and 0.5 mM DTT. (E) Corrected, integrated data, with a curve fit for human platelet profilin−actin data.

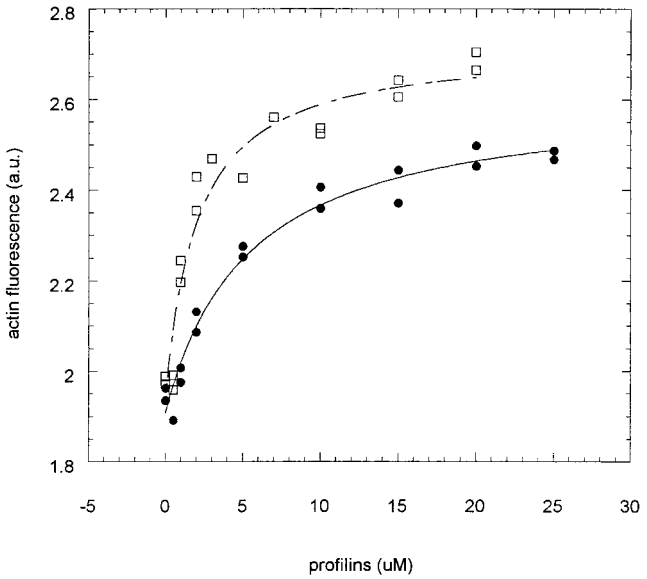

FIGURE 4: Binding of yeast (□) and human (●) profilins to 1 μM pyrene-labeled yeast actin. The increase in pyrene fluorescence intensity due to the binding of profilin was monitored at 385 nm, using excitation at 344 nm.

intrinsic differences in the stability of the profilins, as well as the different buffer conditions utilized.

DISCUSSION

Thermodynamic Analysis of the Profilin−Actin Complex. The actin sequence is very highly conserved among different organisms, and the profilin-binding surface of different actins can thus be expected to be highly conserved. In contrast, the actin binding surface of profilin is weakly conserved (*46*), although the secondary structure elements presented to actin are preserved. On the basis of titration calorimetry, the interactions of yeast and human profilins with rabbit muscle actin are quite different (Table 2). The affinity of yeast profilin ($K_d = 2.9$ μM) for rabbit actin is more than 1 order of magnitude weaker than that of human profilin ($K_d = 0.1$ μM), and the thermodynamic contributions to binding are dissimilar. For the human profilin−rabbit actin interaction, both ΔH and ΔS are favorable, with ΔS providing the majority of the driving force for the reaction. In contrast, for yeast profilin−rabbit actin binding, ΔH is favorable and much larger than the human profilin ΔH, whereas ΔS is unfavorable. The affinity of human profilin for rabbit muscle actin obtained from titration calorimetry is very similar to the reported affinity ($K_d = 0.1-0.2$ μM) of bovine spleen profilin for rabbit muscle actin, as determined by intrinsic fluorescence spectroscopy (*7*), and predicted from indirect methods (*10*).

It is difficult to quantitatively explain differences in binding based on the known crystal structures; however, superposition of the yeast and human profilin structures onto the structure of bovine profilin complexed with actin can

Table 3: Affinities of Pyrene-Labeled Actins for Profilins (K_d in Micromolar)

	yeast profilin	human platelet profilin
yeast actin	2.0 (±0.5)	5.4 (±0.6)
rabbit skeletal muscle actin	18.2 (±6)	2.8 (±1.1)

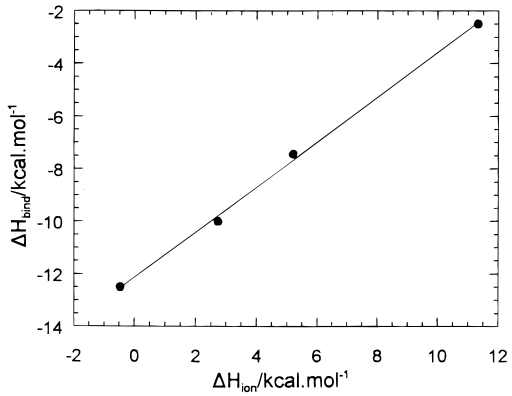

FIGURE 5: Plots of ΔH_{ion} vs ΔH_{bind} for yeast profilin binding to rabbit actin in four different buffers. Values of ΔH_{ion} were obtained from K. Takahashi (personal communication). The slope of the plot gives N_{H^+}, the proton linkage of complex formation, and the intercept gives ΔH_{react}, the intrinsic enthalpy of complex formation. A positive slope indicates that protons are taken up by the complex, whereas a negative slope indicates that protons are released to the buffer on complex formation. Values of ΔH_{ion} for the four buffers are as follows (kcal/mol): Tris, 11.3; MOPS, 5.2; PIPES, 2.73; and cacodylate, −0.47.

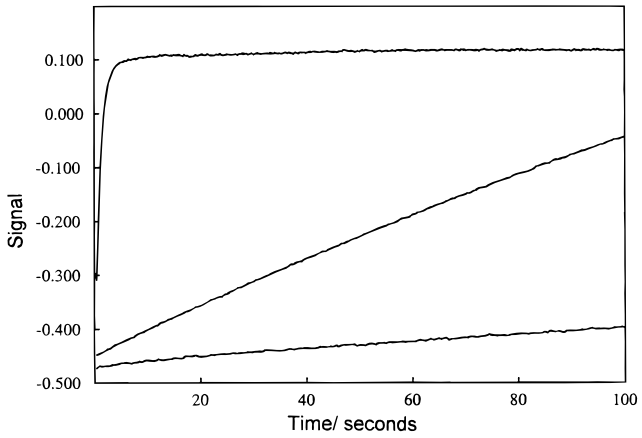

FIGURE 6: Time course of nucleotide exchange from rabbit muscle actin in the absence (lower trace) and presence of 100 μM yeast profilin (middle trace) or 10 μM human platelet profilin (upper trace). The increase in fluorescence intensity due to the binding of ϵATP to 2 μM actin was monitored at wavelengths above 392 nm, using excitation at 360 nm and a 392 nm cutoff filter on the emission.

provide some qualitative insights. As stated above, there is little conservation of profilin residues at the actin−profilin interface. In addition, mammalian profilins have two extended loops between strands β4, β5, and β6 which are five or six residues longer than those observed in other profilins, including yeast profilin, and which contribute residues to the profilin−actin interface. The residues of yeast and human profilin found at the actin−profilin interface are listed in Table 5, along with the interacting actin residues.

In general, favorable entropic contributions to protein−protein association can result from hydrophobic interactions as a consequence of the dehydration of hydrophobic surfaces (i.e., loss of ordered waters). However, the balance of hydrophobic versus polar interactions at the interface is not markedly different in human and yeast profilin. A favorable entropy relies on high complementarity between the associating molecular surfaces; poor complementarity can cause water molecules to be trapped at the interface, resulting in less favorable entropic terms. For example, an unfavorable

Table 4: Kinetics of ATP Dissociation from Yeast and Rabbit Skeletal Muscle Actin

experiment	k_{obs} (s^{-1})
Rabbit Skeletal Muscle Actin	
actin alone	$2.99 \times 10^{-3} \pm 6 \times 10^{-5}$
actin and 100 μM yeast profilin[a]	$8.80 \times 10^{-3} \pm 8 \times 10^{-6}$
actin and 10 μM human profilin[b]	$774 \times 10^{-3} \pm 1 \times 10^{-3}$
Yeast Actin	
actin alone	$6.02 \times 10^{-3} \pm 3.1 \times 10^{-5}$
actin and 100 μM yeast profilin[c]	$1.79 \times 10^{-2} \pm 7.0 \times 10^{-5}$
actin and 40 μM birch profilin[d]	$5.08 \times 10^{-3} \pm 4.2 \times 10^{-5}$
actin and 80 μM birch profilin[d]	$5.38 \times 10^{-3} \pm 6.0 \times 10^{-5}$

[a] Ninety-eight percent of the total actin is estimated to be complexed to profilin. [b] Ninety-nine percent of the total actin is estimated to be complexed to profilin. [c] Ninety-eight percent of the total actin is estimated to be complexed to profilin. [d] N/A, equilibrium dissociation constant not available.

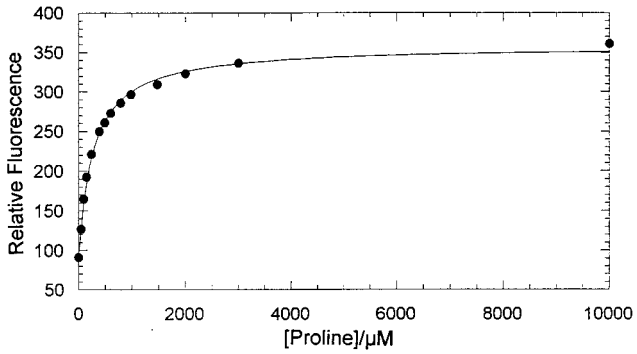

FIGURE 7: Plot of fluorescence intensity vs proline concentration, for addition of Pro_{50} to 2.5 μM yeast profilin. The excitation wavelength was 295 nm (10 nm slit width), and the emission intensity was monitored at 318 nm (3 nm slit width). The curve fit to the data is also shown.

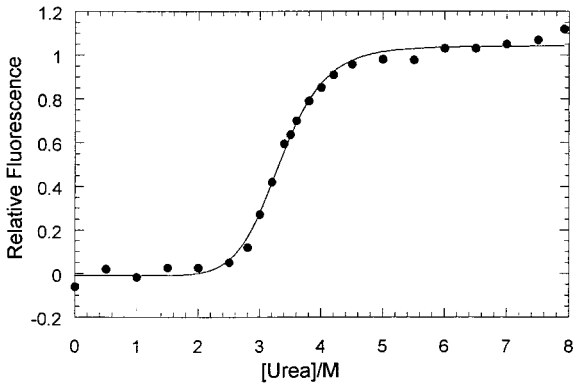

FIGURE 8: Urea denaturation of yeast profilin, monitored by the change in fluorescence intensity at 370 nm with excitation at 295 nm.

entropic contribution to binding has been observed for the formation of the complex between the hen egg white lysozyme antibody D1.3 and lysozyme, where there are many ordered water molecules at the protein−protein interface (*47*). Thus, if the van der Waals surface presented by yeast profilin is less well matched to rabbit actin than the human profilin surface, this could result in a less favorable entropy of binding.

Perhaps harder to explain is the large difference in the enthalpy of yeast and human profilin association with rabbit actin. This could occur if the yeast profilin complex contains a larger number of favorable polar (hydrogen bonding,

Table 5: Amino Acid Residues Found at the Profilin−β-Actin Interface[a]

profilin residue			
yeast	human	bovine	actin residues in contact, description based on the bovine profilin−β-actin complex
Q56	Y59	F59	F59 ring stacks with actin H173; main chain hydrogen bonds to actin D286 (main chain); Y59 of HPP can interact in a similar manner, but the yeast profilin Q56 side chain provides a less hydrophobic interaction; if the Q56 and actin H173 side chains adjust, they could form a hydrogen bond
S57	V60	V60	V60 side chain in van der Waals contact with actin R290 and V287; the main chain is also in contact with actin; in the overlap of profilin structures, S57 is too distant to interact, but if region shifts the side chain could rotate to hydrogen bond with R290, and contact V287 and R290 in a manner similar to that with V60
M68	S71	S71	S71 in van der Waals contact with actin D286 and Y166; M68 is bulkier than serine, suggesting that actin side chains must reorient to accommodate it
L70	I73	I73	carbonyl oxygen of I73 (and L70) is in van der Waals contact with side chain of actin P172, and I73 and L70 side chains are in van der Waals contact with the side chain of actin Y169
R71	R74	R74	side chain makes hydrogen bonds to main chain of actin H371; in the overlay of profilin crystal structures, the arginine side chains display different conformations in each case, but it is predicted that when bound to actin they all adopt the conformation observed in bovine profilin−actin complex
−	E82	E82	residue in long loop, absent in yeast and other lower eukaryotes; E82 hydrogen bonds to actin K113 in bovine complex
S76	S84	T84	T84 is in van der Waals contact with actin R372; S76 and S84 of yeast and human profilin, respectively, display different conformations, but could rotate to provide the same interaction observed in the complex
Y78	D86	D86	D86 side chain is within hydrogen bonding distance of the actin carboxyl terminus, but would need to be protonated to hydrogen bond directly; in the overlay of profilin crystal structures, Y78 is close to both the actin carboxyl terminus and the side chain of actin R372
R80	R88	R88	within van der Waals distance of actin E167 and Y169; yeast R80 is observed in an extended conformation in the native crystal structure, but is likely to reorient when bound to actin so as to assume the same conformation observed in the bovine profilin−actin complex
D82	T97	T97	D82 predicted to be close to actin E167; this residue is at the "tip" of a loop that is much longer in the mammalian profilins, so the nearest mammalian profilin residue is T97, which is ca. 4 Å from actin E167
H81	T89	T89	T89 main chain carbonyl oxygen is in van der Waals contact with actin Y166; H81 is the closest residue in yeast profilin, but is in a somewhat different conformation, resulting in the C_α atom of H81 being closest to actin
−	K90	K90	K90 is within hydrogen bonding of actin D286 and D288; there is no counterpart in yeast profilin, although the K66 ϵ-amino group is close in the yeast profilin structure, and could hydrogen bond to actin D288
G85	N99	N99	in bovine profilin, the N99 side chain is in van der Waals contact with the side chain of actin Y169
Q105	H119	H119	side chain of H119 is within hydrogen bonding distance of actin side chains Y169 and Y133 and the main chain carbonyl oxygen of actin K373; in the human profilin structure, the H119 side chain points in a different direction, but is likely to adopt the same orientation when in complex with actin; similarly, Q105 of yeast profilin could adopt a conformation in the complex which allows hydrogen bonding
A106	G120	G120	hydrogen bond between amide NH and side chain phenolic oxygen of actin Y169
G107	G121	G121	van der Waals contact with actin C-terminal carboxylate, and main chain atoms of actin R372 and K373
T110	N124	N124	N124 can hydrogen bond to side chain of actin R372; T110 of yeast profilin cannot reach to make this interaction
K111	K125	K125	hydrogen bond to actin E361, close to E364; favorable electrostatic interaction
Q115	E129	E129	in van der Waals contact with actin E364; Q115 may be more favorable because there is no charge conflict

[a] Based on the structure of the bovine profilin−β-actin complex, and superposition of the HPP and yeast profilin structures. van der Waals contacts are noted if the distance between interacting atoms is ≤3.8 Å. Hydrogen bonding is noted where donor···acceptor distances are less than 3.3 Å with acceptable geometry.

electrostatic) interactions with actin, by either direct protein−protein interactions or water-mediated interactions. Again, when the superimposed structures are examined, there is no obvious shift toward more polar interactions at the interface, although a few shifts in side chain orientations or different numbers of interfacial waters could account for the difference. A large enthalpic contribution to the overall binding affinity has been observed for the antibody−antigen complex of antibody D1.3 and hen egg white lysozyme, which has a large number of solvent-mediated hydrogen bonds at the antibody−antigen interface (*47*).

Fluorescence titrations using pyrene-labeled rabbit skeletal muscle actin yielded K_d values of 18.2 and 2.8 μM for yeast and human profilins, respectively. Although the absolute affinity for the mammalian proteins determined by this method is 1 order of magnitude weaker than that derived from calorimetry and intrinsic fluorescence, the ratio of the affinities for the yeast and mammalian profilins is similar. The apparently reduced affinity measured by this technique is consistent with other reports (*45*, *48*, *49*), and is likely due to perturbations caused by the pyrene fluorophore. In contrast to the results obtained with mammalian actin,

pyrene-labeled yeast actin bound approximately 2.5-fold more tightly to yeast profilin (K_d = 2.0 μM) than human profilin (K_d = 5.4 μM). These findings suggest that in vivo the stability of the profilin−actin complex may be similar in yeast and mammals. Furthermore, in each case, the cognate profilin−actin complex is more stable than the heterologous complex. This observation suggests that these binding partners have coevolved to achieve the optimal binding interactions required in different organisms and highlights the evolutionary paradigm of coupled molecular evolution.

Proton Linkage. The proton linkage associated with the binding of yeast and human profilin to rabbit actin is significantly different. For yeast profilin binding to rabbit actin, approximately one proton is released by the buffer and taken up by the complex upon complex formation, whereas for human profilin, close to zero protons are taken up by the complex on complex formation. The data do not distinguish whether the proton released from solvent during formation of the yeast profilin−actin complex leads to the protonation of profilin, actin, or a mixture. However, on the basis of the structure of yeast profilin, the sequence differences between yeast and human profilin, and the structure of the bovine actin−profilin complex, we can suggest a likely candidate side chain for protonation.

The fact that a proton is taken up on complex formation at pH 7.2 suggests that the residue involved is probably His, Asp, Glu, or Cys, as Lys and Arg would normally be fully protonated at pH 7.2. It is also likely that if the residue is conserved between human and yeast profilin, then it is not responsible for the protonation observed upon complex formation between yeast profilin and rabbit actin. There are no cysteine residues at the putative yeast profilin−actin interface that have side chains pointing toward the interface. Of the histidine residues at the interface, His173 of actin stacks with Phe59 of profilin in the structure of the bovine profilin−actin complex. In human profilin, Phe59 is replaced by Tyr59, and in yeast profilin, it is Gln56. Protonation of His173 could be required for complex formation with yeast profilin, but it does not appear likely, as the His173 would not need to be protonated to form a hydrogen bond to Gln56, and protonation would bury an uncompensated charge. In fact, it has been previously suggested that in mammalian profilin−actin complexes His173 is likely to be unprotonated at pH 7 (*14*). Of the acidic residues in actin and yeast profilin, there is one good candidate pair of residues for protonation upon complex formation: Asp82 of yeast profilin and Glu167 of rabbit actin. In human profilin, there is no equivalent acidic side chain at this position, and interestingly, in yeast actin, Ala replaces Glu167. It is likely that complex formation between yeast profilin and rabbit actin places these two acidic side chains close to one another, favoring protonation of one of them for removal of the charge−charge interaction and for allowing hydrogen bonding. Other acidic residues at the interface include Asp288 and Asp286 of actin, but neither appears to be an obvious candidate for protonation on complex formation with yeast profilin, as the overall polarity of the neighboring yeast and human profilin residues does not appear to differ significantly, and Asp288 is partly solvent-exposed.

Nucleotide Exchange. The ability of profilin to catalyze the rate of nucleotide exchange on actin has been proposed to play a role in regulating the distribution of G- and F-actin (*8*, *9*, *48*). The rates of nucleotide exchange for rabbit skeletal muscle (2.99×10^{-3} s^{-1}) and yeast (6.02×10^{-3} s^{-1}) actin, under the conditions employed here, are similar within a factor of 2 and are consistent with previously reported values of 7.7×10^{-4} and 5.8×10^{-3} s^{-1} for the mammalian (*49*) and yeast (*50*) actins, respectively. The results in Figure 6 and Table 4 show that there is a significant difference in the abilities of yeast and human profilin to catalyze nucleotide exchange from rabbit skeletal muscle actin. Yeast profilin produces only an approximate 3-fold increase in the rate of nucleotide exchange relative to that of rabbit skeletal muscle actin alone, while human profilin enhances the exchange rate by more than 250-fold. It should be noted that these measurements were taken at concentrations where at least 98% of the total actin should form a 1:1 complex with profilin; under these conditions, near-maximal exchange rates are expected.

Most significantly, yeast profilin is also inefficient in stimulating nucleotide exchange in a homologous system, as it only provides an approximate 3-fold increase in the rate of nucleotide exchange relative to that of yeast actin alone. The relatively low nucleotide exchange activity of yeast profilin with yeast actin indicates that this mechanism may not play a major role in regulating the actin cytoskeleton in *S. cerevisiae*. The concentration of yeast profilin used, 100 μM, is likely to represent an excess over the in vivo concentration of yeast profilin, suggesting that the actual extent of profilin-associated nucleotide exchange in vivo is lower than that reported here. This proposal is consistent with the report that *Arabidopsis* profilin can effectively complement the *S. cerevisiae* profilin null (*51*), despite the fact that *Arabidopsis* profilin lacks actin nucleotide exchange activity on rabbit skeletal muscle actin (*52*) and that another plant profilin, birch pollen profilin, shows no enhancement of nucleotide exchange on yeast actin (Table 4). Taken together, these findings support a minor role for profilin-catalyzed adenine nucleotide exchange in yeast; however, the role of this activity in mammalian systems is not ruled out.

*Poly-*L*-proline Binding Site.* The poly-L-proline binding site of profilins has been identified as a highly conserved patch of hydrophobic residues on the surface of the molecule, composed of Trp2, Tyr5, Trp29, Tyr119, and Tyr125 in yeast profilin (*17*−*21*). The affinity of yeast profilin for Pro_{50} (K_d = 276 μM per proline) is similar to the reported affinity of *Acanthamoeba* binding to Pro_{80} (K_d = 120 μM per proline; *42*). These two profilins have completely conserved poly-L-proline binding sites, except for the substitution of Tyr125 in yeast for Phe125 in *Acanthamoeba* profilin. Superposition of the *Acanthamoeba* and yeast profilin (molecule A) with the human platelet profilin bound to a decamer of L-proline (*21*) shows a close correspondence of the poly-L-proline binding sites (Figure 9), with an rms difference of 1.9 Å for all superimposable atoms of the poly-L-proline interacting residues of *Acanthamoeba* and yeast profilin. This structural similarity is consistent with the observed poly-L-proline binding affinities and indicates that all cellular profilins bind proline-rich peptides in a similar manner.

Interpretation of S. cerevisiae Profilin Mutants. The structure of yeast profilin presented in this paper provides a framework for understanding the effects of profilin mutations

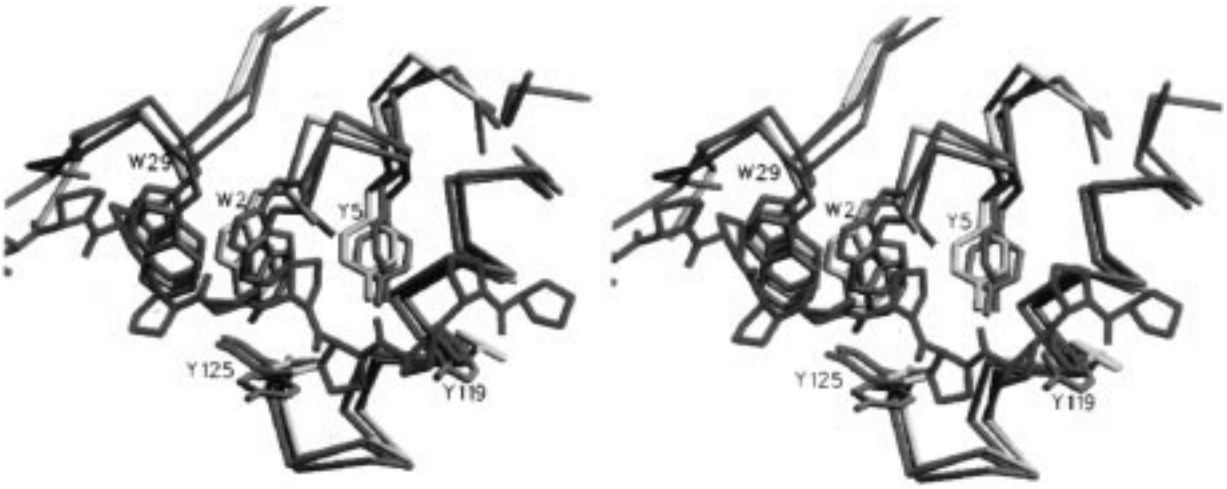

FIGURE 9: Overlay of poly-L-proline binding sites for yeast (pink), human (blue), and *Acanthamoeba* (yellow) profilins, with the poly-L-proline (Pro_{10}) structure bound to human profilin also shown (green).

and for integrating the results obtained from genetic, biochemical, and physical approaches (*1*, *12*). Truncations of three to eight residues at the C terminus of yeast profilin are reported to have effects of increasing severity on the integrity of the actin cytoskeleton and the ability of profilin to bind poly-L-proline (*12*). Deletion of the last three residues of the C terminus, which includes Tyr125 of the poly-L-proline binding site (Figure 9), reduced but did not eliminate binding to poly-L-proline, and produced only minor effects on the actin cytoskeleton. Removal of seven or eight residues from the C terminus of profilin, including Tyr119 and Tyr125, abolished poly-L-proline binding and resulted in very severe cytoskeletal defects. These results are consistent with the existing structural data (*21*) regarding the poly-L-proline binding site, as the deletion of Tyr125 alone may be expected to impair but not necessarily abolish poly-L-proline binding. The deletion of six or more residues removes two of the five aromatic residues which form the poly-L-proline binding site and therefore might be expected to greatly diminish or completely eliminate binding. All of the truncation mutants bind actin, consistent with the structure of the profilin−actin complex (*14*) showing that the deleted residues do not participate in the actin binding interface. Similarly, C-terminal truncations of *Acanthamoeba* profilin also retain actin binding activity (*18*). These findings suggest that the severe cytoskeletal phenotypes associated with the longer truncation mutants result, at least in part, from impaired binding to proline-rich ligands and that this activity is an important in vivo function of profilin. This is consistent with the observation that the poly-L-proline binding site is the most highly conserved region in the profilin family (*46*).

Mutations of basic residues proposed to comprise the PIP_2 binding site in yeast profilin were found to have more significant effects than the C-terminal truncations on in vitro actin binding and the integrity of the actin cytoskeleton (*1*, *12*). These observations support the hypothesis that PIP_2 and actin share overlapping binding sites on the profilin molecule (*12*−*14*). Mutation of Arg71 to Glu, or Arg80 to Gly, results in reduced actin binding, whereas mutation of Arg75 to Gly does not affect actin binding. These observations are consistent with the crystal structure, which shows that both Arg71 and Arg80 contribute to the actin binding site (see Table 5), whereas Arg75 is more distant from the actin binding site, being about 5 Å from actin residue Arg372. Mutation of Arg71 to Glu was observed to give rise to in vivo defects that are similar to, albeit less severe, than those for deletion of the profilin gene and supports the role of this residue in stabilizing the actin−profilin complex. The combined genetic, biochemical, and structural data suggest that in yeast, normal morphology and growth require profilin to participate in productive interactions with both actin and proline-rich ligands.

ACKNOWLEDGMENT

We thank Dr. Michael Toney for help with the stopped-flow kinetic experiments.

REFERENCES

1. Haarer, B. K., Lillie, S. K., Adams, A. E. M., Magdolen, V., Bandlow, W., and Brown, S. S. (1990) *J. Cell. Biol. 110*, 105−114.
2. Cooley, L., Verheyen, E., and Ayers, K. (1992) *Cell 69*, 173−184.
3. Balasubramanian, M. K., Hirani, B. R., Burke, J. D., and Gould, K. L. (1994) *J. Cell. Biol. 125*, 1289−1301.
4. Finkel, T., Theriot, J. A., Dise, K. R., Tomasell, G. F., and Goldschmidt-Clermont, P. J. (1994) *Proc. Natl. Acad. Sci. U.S.A. 91*, 1510−1514.
5. Pollard, T. D., and Cooper, J. A. (1986) *Annu. Rev. Biochem. 55*, 987−1035.
6. Pring, M., Weber, A., and Bubb, M. R. (1992) *Biochemistry 31*, 1827−1836.
7. Perelroizen, I., Marchand, J., Blanchoin, L., Didry, D., and Carlier, M.-F. (1994) *Biochemistry 33*, 8472−8478.
8. Goldschmidt-Clermont, P. J., Furman, M. I., Wachsstock, D., Safer, D., Nachmias, V. T., and Pollard, T. D. (1992) *Mol. Cell. Biol. 3*, 1015−1024.
9. Carlier, M. F., Jean, C., Rieger, K. J., Lenfant, M., and Pantaloni, D. (1993) *Proc. Natl. Acad. Sci. U.S.A. 90*, 5034−5038.
10. Pantaloni, D., and Carlier, M.-F. (1993) *Cell 75*, 1007−1014.
11. Lassing, I., and Lindberg, U. (1985) *Nature 318*, 472−474.
12. Haarer, B. K., Petzold, A. S., and Brown, S. S. (1993) *Mol. Cell. Biol. 13*, 7864−7873.
13. Fedorov, A. A., Magnus, K. A., Graupe, M. H., Lattman, E. E., Pollard, T. D., and Almo, S. C. (1994) *Proc. Natl. Acad. Sci. U.S.A. 91*, 8636−8640.
14. Schutt, C. E., Myslik, J. C., Rozycki, M. D., Goonesekere, N. C. W., and Lindberg, U. (1993) *Nature 365*, 810−816.

15. Goldschmidt-Clermont, P. J., Kimm, P. J., Machesky, L. M., Rhee, S. G., and Pollard, T. D. (1991) *Science 251*, 1231−1233.
16. Singh, S. S., Chauhan, A., Murakami, N., and Chauhan, V. P. S. (1996) *Biochemistry 35*, 16544−16549.
17. Björkegren, C., Rozycki, M., Schutt, C. E., Lindberg, U., and Karlsson, R. (1993) *FEBS Lett. 333*, 123−126.
18. Kaiser, D., and Pollard, T. D. (1996) *J. Mol. Biol. 256*, 89−107.
19. Archer, S. J., Vinson, V. K., Pollard, T. D., and Torchia, D. A. (1994) *FEBS Lett. 337*, 145−151.
20. Metzler, W. J., Bell, A. J., Ernst, E., Lavoie, T. B., and Mueller, L. (1994) *J. Biol. Chem. 269*, 4620−4625.
21. Mahoney, N. M., Janmey, P. A., and Almo, S. C. (1997) *Nat. Struct. Biol. 4*, 953−960.
22. Reinhard, M., Geihl, K., Abel, K., Haffner, C., Jarchau, T., Hoppe, V., Jockusch, B. M., and Walter, U. (1995) *EMBO J. 14*, 1583−1589.
23. Chakraborty, T., Ebel, F., Domann, E., Niebuhr, K., Gerstel, B., Pistor, S., Temm-Grove, C. J., Jockusch, B. M., Reinhard, M., and Walter, U. (1995) *EMBO J. 14*, 1314−1321.
24. Gertler, F. B., Niebuhr, K., Reinhard, M., Wehland, J., and Soriano, P. (1996) *Cell 87*, 227−239.
25. Evangelista, M., Blundell, K., Longtine, M. S., Chow, C. J., Adames, N., Pringle, J. R., Peter, M., and Boone, C. (1997) *Science 276*, 118−122.
26. Chang, F., Drubin, D., and Nurse, P. (1997) *J. Cell. Biol. 137*, 169−182.
27. Imamura, H., Tanaka, K., Hihara, M., Umikawa, M., Kamei, T., Takahashi, K., Sasaki, T., and Takai, Y. (1997) *EMBO J. 16*, 2745−2755.
28. Watanabe, N., Madule, P., Reid, T., Ishizaki, T., Watanabe, G., Kakizuka, A., Saito, Y., Nakao, K., Jockusch, B. M., and Narumiya, S. (1997) *EMBO J. 16*, 3044−3056.
29. Adams, A. E., and Pringle, J. R. (1984) *J. Cell Biol. 98*, 934−945.
30. Kilmartin, J. V., and Adams, A. E. (1984) *J. Cell Biol. 98*, 922−933.
31. Fedorov, A. A., Pollard, T. D., and Almo, S. C. (1994) *J. Mol. Biol. 241*, 480−482.
32. Fedorov, A. A., Ball, T., Mahoney, N. M., Valenta, R., and Almo, S. C. (1997) *Structure 5*, 33−45.
33. Spudich, J. A., and Watt, S. (1971) *J. Biol. Chem. 246*, 4866−4871.
34. Lee, S., Li, M., and Pollard, T. D. (1988) *Anal. Biochem. 168*, 148−155.
35. Cook, R. K., Blake, W. T., and Rubenstein, P. A. (1992) *J. Biol. Chem. 267*, 9430−9436.
36. Kabsch, W. (1988) *J. Appl. Crystallogr. 21*, 916−924.
37. Howard, A. J. (1986) *A guide to data reduction for the Nicolet imaging proportional counter: the XENGEN system*, Genex Corp., Gaithersburg, MD.
38. Navaza, J. (1994) *Acta Crystallogr. A50*, 157−163.
39. Collaborative Computational Project Number 4 (1994) *Acta Crystallogr. D50*, 760−763.
40. Brünger, A. T. (1992) *X-PLOR, version 3.1: a system for X-ray crystallography and NMR*, Yale University Press, New Haven, CT.
41. Jones, T. A., Zou, J.-Y., Cowan, S. W., and Kjeldgaard, M. (1991) *Acta Crystallogr. A47*, 110−119.
42. Petrella, E. C., Machesky, L. M., Kaiser, D. A., and Pollard, T. D. (1996) *Biochemistry 35*, 16535−16543.
43. Cedergren-Zeppezauer, E. S., Goonesekere, N. C. W., Rozycki, M. D., Myslik, J. C., Dauter, Z., Lindberg, U., and Schutt, C. E. (1994) *J. Mol. Biol. 240*, 459−475.
44. Murphy, K. P., Xie, D., Garcia, K. C., Amzel, L. M., and Freire, E. (1993) *Proteins: Struct., Funct., Genet. 15*, 113−120.
45. Almo, S. C., Pollard, T. D., Way, W., and Lattman, E. E. (1994) *J. Mol. Biol. 236*, 950−952.
46. Thorn, K. S., Christensen, E. M., Shigeta, R., Huddler, D., Shalaby, L., Lindberg, U., Chua, N.-H., and Schutt, C. E. (1997) *Structure 5*, 19−32.
47. Bhat, T. N., Bentley, G. A., Boulot, G., Greene, M. I., Tello, D., Dall'Acqua, W., Souchon, H., Schwarz, F. P., Mariuzza, R. A., and Poljak, R. J. (1994) *Proc. Natl. Acad. Sci. U.S.A. 91*, 1089−1093.
48. Goldschmidt-Clermont, P. J., Machesky, L. M., Doberstein, S. K., and Pollard, T. D. (1991) *J. Cell Biol. 113*, 1081−1089.
49. Mockrin, S. C., and Korn, E. D. (1980) *Biochemistry 19*, 5359−5362.
50. Chen, X., Cook, R. K., and Rubenstein, P. A. (1993) *J. Cell Biol. 123*, 1185−1195.
51. Christensen, H. E. M., Ramachandran, S., Tan, C.-T., Surana, U., Dong, C.-H., and Chua, N.-H. (1996) *Plant J. 10*, 269−279.
52. Perelroizen, I., Didry, D., Christensen, H., Chua, N.-H., and Carlier, M.-F. (1996) *J. Biol. Chem. 271*, 12302−12309.

BI9720033